

# In-gap States and Carrier Recombination in Quasi-2D Perovskite Films

Bat-El Cohen, Ron Alafi, Jonathan Beinglass, Adva Shpatz Dayan, Oren Goldberg, Shachar Gold, Isaac Balberg, Leeor Kronik, Lioz Etgar, Oded Millo, and Doron Azulay\*

In-gap states and their effect on recombination rates in quasi-2D lead-iodide-based perovskites, intercalated with various spacer molecules, are studied using a combination of scanning tunneling spectroscopy and temperature-dependent photoconductivity measurements. The results are further analyzed by a Shockley–Read–Hall model. Indications for shallow in-gap states, positioned at about 0.15–0.2 eV below the bottom of the conduction band, are found. These states are identified as dominating the recombination route of photogenerated carriers in these systems, with a relatively large capture coefficient of about  $10^{-5}$ – $10^{-6}$  cm<sup>3</sup> s<sup>-1</sup> at room temperature. First-principles calculations based on density functional theory imply that these states are not an intrinsic effect of the inclusion of the spacer molecules, but rather one that arises from chemical defect formation or structural deformation of the perovskite layers. The results suggest that further improvement of the performance of solar cells that are based on quasi-2D perovskites requires, along with enhancing carrier mobility, efforts to suppress the concentration of these detrimental defect states.

reduce their mobility. Many efforts have been made to overcome this limitation by using special deposition techniques, such as hot-casting<sup>[2]</sup> or chemical modifications.<sup>[3–7]</sup> Another major factor that influences the performance of a solar cell is the recombination kinetics of the photogenerated carriers, which is governed by the density of recombination centers in the material, their energetic position, and their capture coefficients. While there are numerous theoretical and experimental studies on the formation and passivation of defects in 3D halide perovskites—see, e.g., refs. [8–16]—there are fewer such investigations on low-dimensional perovskites—see, e.g., refs. [17–20]. Such studies are highly lacking, in particular in relation to the formation of in-gap states and their effect on the photoelectronic properties of these systems that, in turn, affect the performance of corresponding solar-cell devices.

In this work, we investigate the formation of in-gap states in quasi-2D ( $n = 5$ ) lead-iodide-based perovskites, intercalated with various spacer molecules, and their influence on the recombination kinetics and photoconductivity. To study the properties of the different perovskite films, we employed scanning tunneling spectroscopy (STS), temperature-dependent photoconductivity measurements, photoluminescence (PL) and absorption spectroscopies, as well as density functional theory (DFT) calculations. We also analyzed the temperature dependence of the photoconductivity, considering the tunneling and optical spectroscopy data, using the Shockley–Read–Hall (SRH) model with one effective recombination level.

## 1. Introduction

Quasi-2D perovskites have been receiving significant attention, primarily owing to their improved stability in comparison with their 3D counterparts.<sup>[1]</sup> In these structures, with the general formula of  $(\text{R-NH}_3)_2(\text{MA})_{n-1}\text{Pb}_n\text{I}_{3n+1}$ , the perovskite layers are surrounded by organic spacer molecules, usually mono- or divalent organic cations. These shield the metal halide octahedra, e.g., by forming a hydrophobic barrier, and thus improve the stability of the films against humidity. However, the insertion of such molecules may influence the electronic properties of the films. For example, the organic spacer molecules can form a barrier for charge carriers and thus

B.-E. Cohen, A. Shpatz Dayan, L. Etgar  
Institute of Chemistry  
Casali Center for Applied Chemistry and the Center for Nanoscience and Nanotechnology  
The Hebrew University of Jerusalem  
Jerusalem 9190401, Israel

 The ORCID identification number(s) for the author(s) of this article can be found under <https://doi.org/10.1002/solr.202300813>.

© 2023 The Authors. Solar RRL published by Wiley-VCH GmbH. This is an open access article under the terms of the Creative Commons Attribution-NonCommercial-NoDerivs License, which permits use and distribution in any medium, provided the original work is properly cited, the use is non-commercial and no modifications or adaptations are made.

DOI: 10.1002/solr.202300813

R. Alafi, D. Azulay  
Azrieli College of Engineering  
Jerusalem 9103501, Israel  
E-mail: azulay.doron@mail.huji.ac.il

J. Beinglass, O. Goldberg, I. Balberg, O. Millo, D. Azulay  
Racah Institute of Physics  
The Hebrew University of Jerusalem  
Jerusalem 9190401, Israel

S. Gold, L. Kronik  
Department of Molecular Chemistry and Materials Science  
Weizmann Institute of Science  
Rehovoth 7610001, Israel

## 2. Results and Discussion

### 2.1. Fabrication and Optical Characterization of Quasi-2D Perovskite Films

It is well accepted that the structure of the barrier molecule has a major effect on the perovskite properties. For example, perovskite films prepared using an aromatic barrier are more stable than those prepared with the linear counterpart.<sup>[21]</sup> Furthermore, the structure of the perovskite is also dictated by the character of the barrier molecule; the monoammonium barriers usually form in the Ruddlesden–Popper phase of the perovskite, while the diammonium barrier typically forms in the Dion–Jacobson phase (Figure 1b,c). The stability of the perovskite film and the photovoltaic properties of the devices are influenced by the perovskite phase as well.<sup>[1]</sup>

Following these considerations, four types of representative barrier (or spacer) cation molecules were chosen, maintaining different functionalities—aromatic, linear, monoammonium, and diammonium. These are benzylammonium (BnzA), butylammonium (BuA), 1,4-butanediammonium (BuDA), and 1,4-benzenedimethan ammonium (BnzDA). A schematic illustration of these cations can be found in Figure 1a.

To evaluate the photoelectronic properties of the low dimensional perovskite films, we fabricated  $n = 5$  samples, i.e.,

following the chemical formulas of  $(R-NH_3)_2(MA)_4Pb_5I_{16}$  and  $(NH_3-R-NH_3)(MA)_4Pb_5I_{16}$ , where MA is methyl-ammonium, R-NH<sub>3</sub> is BuA or BnzA, and NH<sub>3</sub>-R-NH<sub>3</sub> is BnzDA or BuDA. The films were fabricated by solution deposition, where the starting perovskite solutions were prepared according to the stoichiometric ratio of the perovskite components.

Figure 2a shows absorption spectra obtained from the films studied in this work. The absorption edge found for all samples was about 1.6 eV, similar to that of the 3D sample. These results were further corroborated by the PL spectra, shown in Figure 1b, which indicate an energy gap in the range 1.6–1.64 eV, with small shifts between different spacer molecules, as previously reported.<sup>[4,7]</sup>

### 2.2. Tunneling Spectroscopy and Photoconductivity Characterization

To study experimentally the influence of the different spacer (barrier) molecules on the density of states (DOS) of the quasi-2D perovskite ( $n = 5$ ) considered in this work, we employed STS measurements. Figure 3a shows typical  $dI/dV$ - $V$  tunneling spectra, measured on samples containing the different spacer molecules. All spectra display an energy gap of about 1.6 eV, with small deviations between the different films, in agreement with the optical measurements. In Figure 3a, only

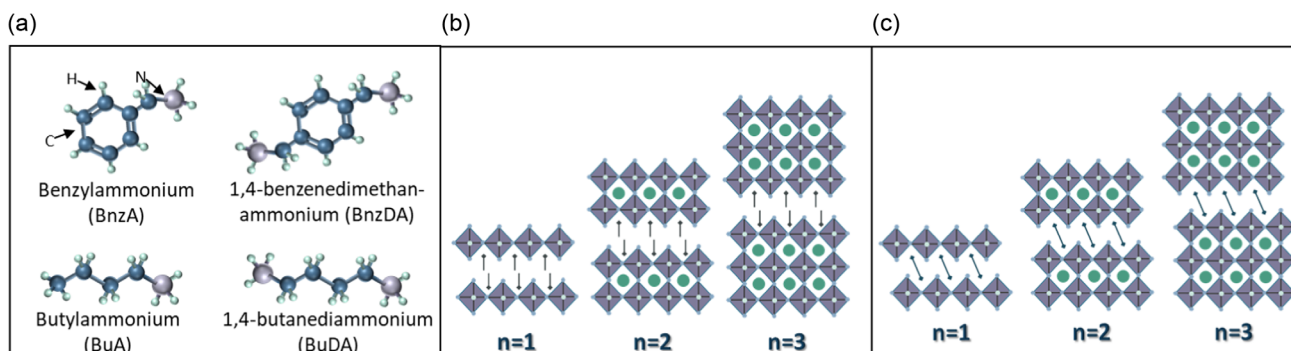


**Figure 1.** Schematic illustration of a) the barrier molecules used for the fabrication of low-dimensional perovskite films studied here; b) monoammonium-based Ruddlesden–Popper  $[(R-NH_3)_2(MA)_{n-1}Pb_nI_{3n+1}]$  and c) diammonium-based Dion–Jacobson  $[NH_3-R-NH_3](MA)_{n-1}Pb_nI_{3n+1}]$  phases of two-dimensional perovskites using the barrier molecules.

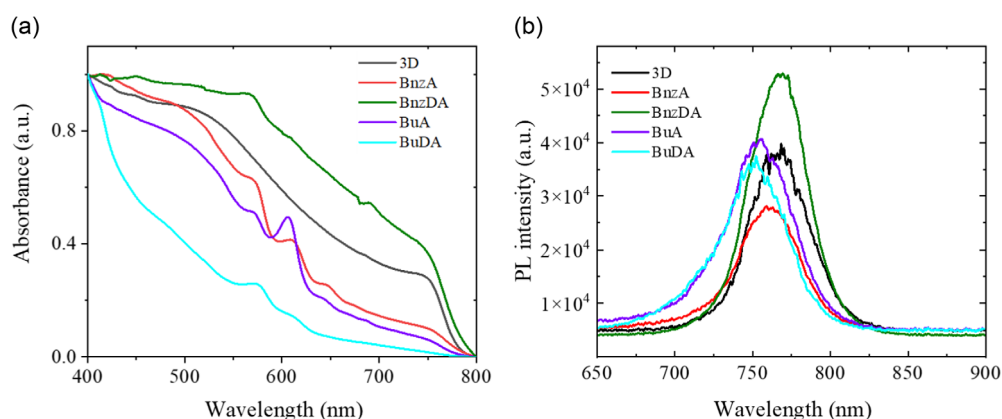


**Figure 2.** a) Absorption and b) PL spectra obtained from the different (3D and quasi-2D with different barrier molecules) perovskite films.

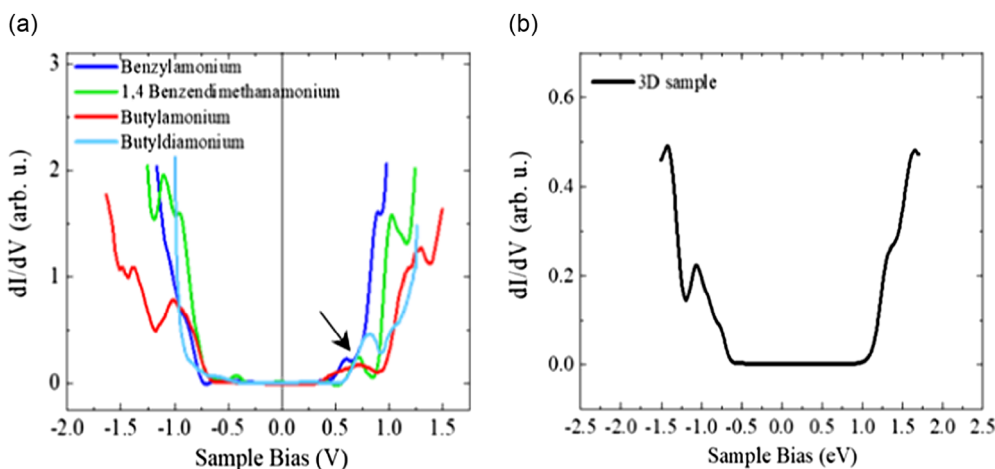


**Figure 3.** a)  $dI/dV$ -V tunneling spectra, measured on quasi-2D ( $n = 5$ ) perovskite films with different spacer molecules. All films exhibit indications for shallow in-gap states below the conduction band edge. The arrow points to the energetic region of the in-gap states. b)  $dI/dV$ -V tunneling spectrum measured on a 3D film. Note the absence of in-gap states.

small changes in the position of the Fermi energy (zero bias in the spectra) relative to the valence band edge are observed. These changes in the position of the Fermi energy resemble the results reported by Phuyal et al.<sup>[22]</sup> for  $\text{PbI}_2$ -based 2D perovskites with different dialkylammonium cations, where they have been attributed mainly to structural changes. Importantly, for all four molecules, there is a clear indication of the presence of shallow electronic levels within the energy gap, positioned at 0.15–0.2 eV below the conduction band edge. These levels are absent in a corresponding spectrum measured on a 3D reference sample, as shown in Figure 3b.

A major question is the influence of the observed in-gap states on the recombination kinetics of photogenerated carriers. To assess it, we measured the photoconductivity of the above films as a function of temperature and illumination intensity. The results, presented in Figure 4, show that for all spacer molecules, the photoconductivity increases with temperature. This behavior is consistent with the dominance of a shallow recombination level,<sup>[23,24]</sup> in agreement with the STS results.

To further relate the dominant recombination route to the in-gap states found by the STS measurements, we analyzed the photoconductivity results within the framework of the SRH model, using a single effective recombination level. Briefly, this model is described by the following set of equation<sup>[24–26]</sup>

$$G = C_n(N_r - n_r)n - C_n n_r N_C \exp\left[-\frac{E_C - E_r}{kT}\right] \quad (1a)$$

$$G = C_p n_r p - C_p(N_r - n_r)N_V \exp\left[-\frac{E_r - E_V}{kT}\right] \quad (1b)$$

and the charge neutrality condition

$$(p - p_0) = (n - n_0) + (n_r - n_{r_0}) \quad (2)$$

where,  $n$ ,  $p$ , and  $n_r$  represent the concentration of the electrons, holes, and occupied recombination centers (respectively) under illumination (with the subscript 0 denoting dark quantities).  $N_r$  is the overall density of the recombination centers at an energy level

$E_r$ .  $C_n$  and  $C_p$  are the capture coefficients of the centers for electrons and holes.  $G$  represents the electron/hole generation rate. By solving the above equations, one can express the photoconductivity of the system, defined by  $\sigma_{\text{photo}} = q(\mu_n \Delta n + \mu_p \Delta p)$ , and fit it to our experimental results. In this expression,  $q$  is the electron charge,  $\Delta n = (n - n_0)$ ,  $\Delta p = (p - p_0)$ , and  $\mu_n$  and  $\mu_p$  are the electron and hole mobilities, respectively.

In the fitting procedure, we first estimated some of the parameters involved in the model. The energy gap of the films, as well as the position of the Fermi energy and the recombination levels, were deduced from the PL and STS results. The majority carrier mobilities under illumination at room temperature were estimated from photo-Hall measurements, showing Hall mobility in the range of  $3.7\text{--}10 \text{ cm}^2 \text{ V}^{-1} \text{ s}^{-1}$  for the different barriers. From these mobility values and the dependence of photoconductivity on the illumination intensity in the intensity range where  $p \approx \sqrt{\frac{G}{C_p}}$ ,<sup>[3]</sup> we roughly estimated the magnitude of the hole capture coefficients at room temperature using  $\sigma_{\text{photo}} = q\mu_p p \approx q \frac{\mu_p}{\sqrt{C_p}} \sqrt{G}$ . We found it to be quite large, about  $10^{-5}\text{--}10^{-6} \text{ cm}^3 \text{ s}^{-1}$ . Additionally, by analyzing the photoconductivity as a function of the illumination intensity (i.e., the generation rate,  $G$ ) at the intensity range where  $\sigma_{\text{photo}} \propto \sqrt{G}$ , one can extract the value of  $\mu_p/\sqrt{C_p}$ , as illustrated in Figure 5 for the BnzDA sample at 270 K. Using this procedure, we estimated the temperature dependence of  $\mu_p^2/C_p$ .<sup>[3]</sup> This dependence imposes another restriction on our fitting procedure. As shown in Figure 4 (blue lines), the results of the above fitting procedure to the SRH model are in good agreement with the experimental data, implying that the in-gap states found in our STS measurements are correlated to the dominant recombination centers in the perovskite films. This could be one of the reasons for the relatively low conversion efficiencies found for solar cells that are based on such quasi-2D perovskites, which means that the ability to reduce the density of such defects may be crucial to further improvement in the performance of the corresponding solar cells.

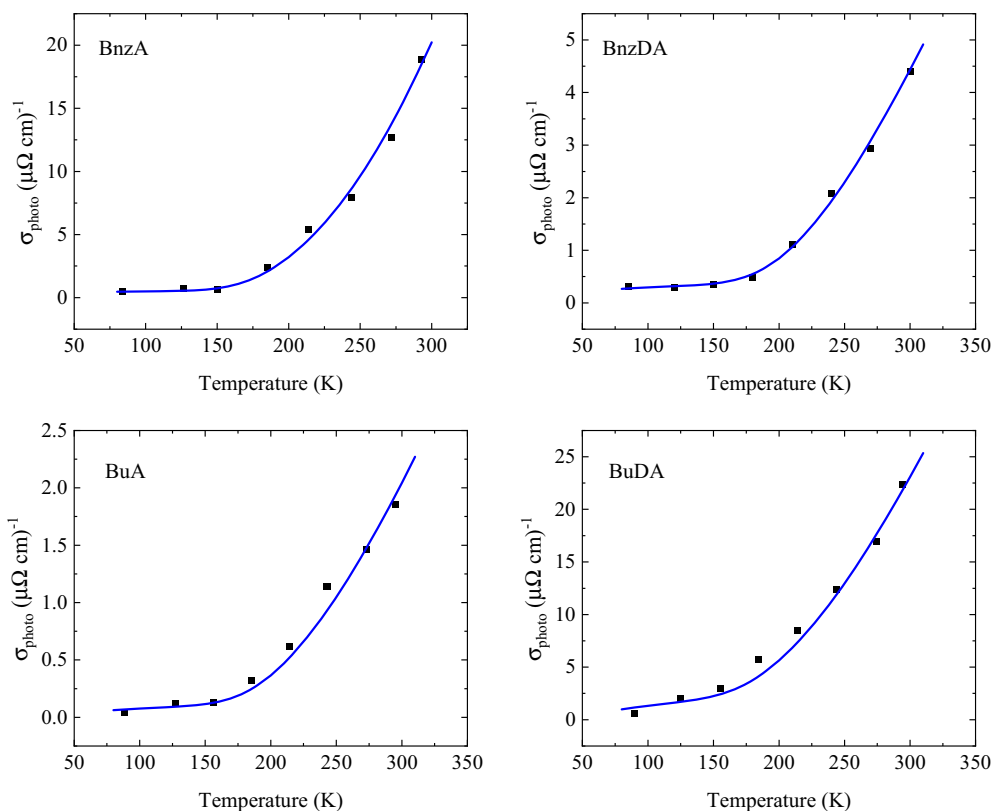


**Figure 4.** Photoconductivity as a function of temperature for perovskite films ( $n = 5$ ) with different spacer molecules (black dots). Blue solid lines—fit to the SRH model. See text for details.

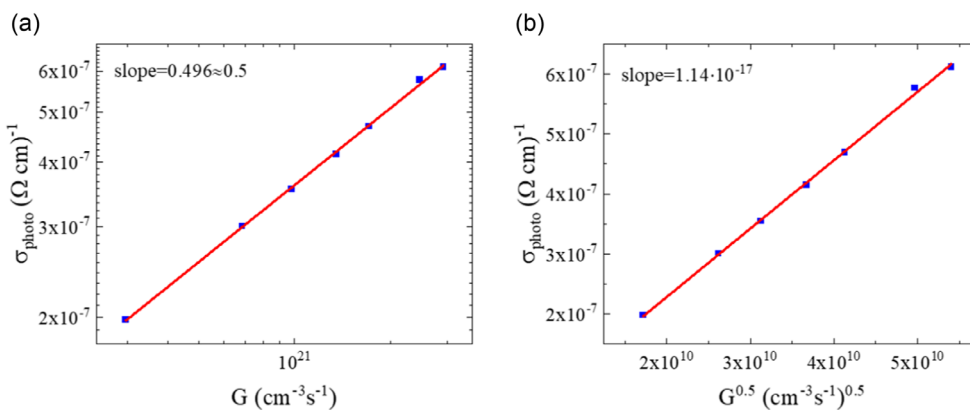


**Figure 5.** a) Photoconductivity as a function of generation rate ( $G$ ) of the BnzDA sample at 270 K. Note the relation  $\sigma_{\text{photo}} \propto \sqrt{G}$ . b) Photoconductivity as a function of  $\sqrt{G}$ , indicating  $\mu_p / \sqrt{C_p} = 71.3 \left(\frac{\text{cm}}{\text{V}^2 \text{s}}\right)^{1/2}$ .

### 2.3. Evolution of In-gap States with Dimensionality

As mentioned above, the dimensionality of the films may also affect their DOS. To understand the nature of this influence, we measured a series of samples with butylammonium spacer molecules with  $n = 1, 5, 7,$  and  $10$  using STS. The results, shown in **Figure 6**, indicate that for  $n = 1$  (**Figure 6a**), there are two in-gap state distributions, one close to the conduction band and one closer to the valence band edges. As  $n$  increases, the

states close to the valence band edge vanish (already for  $n = 5$ ; **Figure 6b**). Moreover, as  $n$  further increases (**Figure 6c**,  $n = 7$ ), the states close to the conduction band edge are further pushed into the conduction band and eventually disappear for  $n = 10$  (**Figure 6d**). This behavior implies a possible relation between the appearance of these in-gap states and the quantum confinement effect in the films. Specifically, it could be that defect states that usually reside above the bottom of the conduction band or below the top of the valence band in the 3D material,

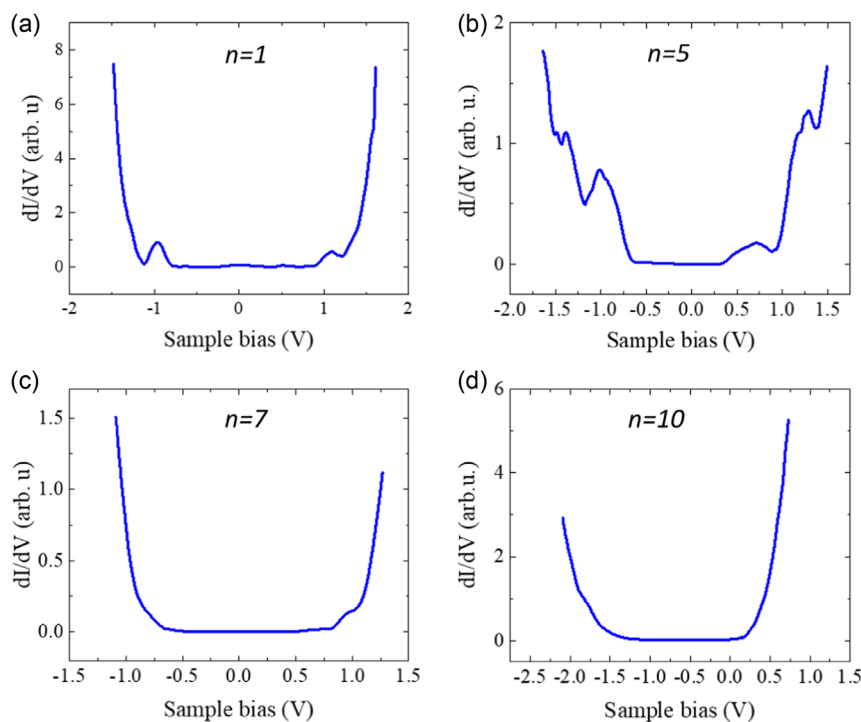


**Figure 6.**  $dI/dV$ - $V$  tunneling spectra measured on  $n = 1, 5, 7,$  and  $10$  perovskite films with butylammonium spacer molecules, showing the evolution of the in-gap state distribution with increasing  $n$ .

become in-gap states in low  $n$  films due to quantum confinement and might serve as recombination centers. As  $n = 1$  partial density of states calculations, shown in **Figure 7**, rule out a direct molecular contribution, the behavior may have to do with defects, in which case the molecular dependence can be attributed to the interaction of semiconductor defect states with molecular levels.<sup>[27]</sup> Another possibility is that the formation of these states is related to an indirect effect of molecule-induced structural deformation or chemical modification that is more pronounced at low dimensionality.

#### 2.4. Influence of the Spacer Molecules on the DOS of the Films—A DFT Study

To examine whether the barrier molecules contribute to the formation of the in-gap states directly, we have calculated the partial density of states (pDOS) reflecting the contribution of each atomic species. All calculations were based on the Perdew–Burke–Ernzerhof (PBE)<sup>[28]</sup> approximate exchange–correlation functional within DFT, augmented by Tkatchenko–Scheffler dispersion terms with iterative Hirshfeld partitioning,<sup>[29,30]</sup> as implemented in the VASP plane-wave software suite.<sup>[31,32]</sup> We have relied on structures available in the literature where possible (BnzA, BuA, and BuDA)<sup>[3,33]</sup> and based on a reasonable chemical bonding scenario else (BnzDA). Throughout, we have used  $n = 1$ , because the effect of in-gap states is expected to be most pronounced in this case (an issue elaborated below), and also owing to the computational cost involved. We note that a previous study<sup>[18]</sup> has focused on  $n = 1–3$  and found the presence of

the effect regardless of  $n$ . All systems were relaxed using a  $k$ -point grid of  $8 \times 8 \times 1$  for the BnzDA,  $5 \times 5 \times 1$  for the BuA and BnzA, and  $5 \times 5 \times 5$  for the BuDA molecular spacers, with an energy cutoff of 950 eV for all systems. Post relaxation, spin-orbit coupling was used in the final electronic structure calculations.

We found that the computed perovskite bandgap energies are relatively close for all systems, at  $\approx 1.5$  eV. The bandgap of the BnzDA system was somewhat smaller, at 1.43 eV (perhaps a consequence of its computed structure). Note that these values underestimate the experimental ones, a well-known issue within DFT,<sup>[34]</sup> but trends can still be well captured. pDOS results for the four structures considered experimentally are shown in **Figure 7a–d**. Clearly, there is no significant contribution of the organic molecule to the near-band-edge DOS of the overall system, as the states found at the band edges are dominated by the species of the inorganic perovskite layer (namely, iodide and lead). The dominant factor for the molecular pDOS appears to be the number of amines, as the pDOS for the lead and iodine near the band edges in the two monoamine systems is similar, but different from that of the diamine systems (even though, as expected, far from the band edges the carbon pDOS for the benzene-analog systems are more similar to each other than to those of the butane-analog systems). This conclusion differs from that of a previous study involving bimidazolium (IMI),<sup>[18]</sup> where molecular gap states were identified. This difference is not a technical issue, as we have reproduced the computational results of that study as part of our own work, see **Figure 7e**. Our results do agree well with a different earlier study, which noted that organic contributions to the DOS arise only when the amine group is part of an aromatic system for diamine systems.<sup>[19]</sup> It also agrees

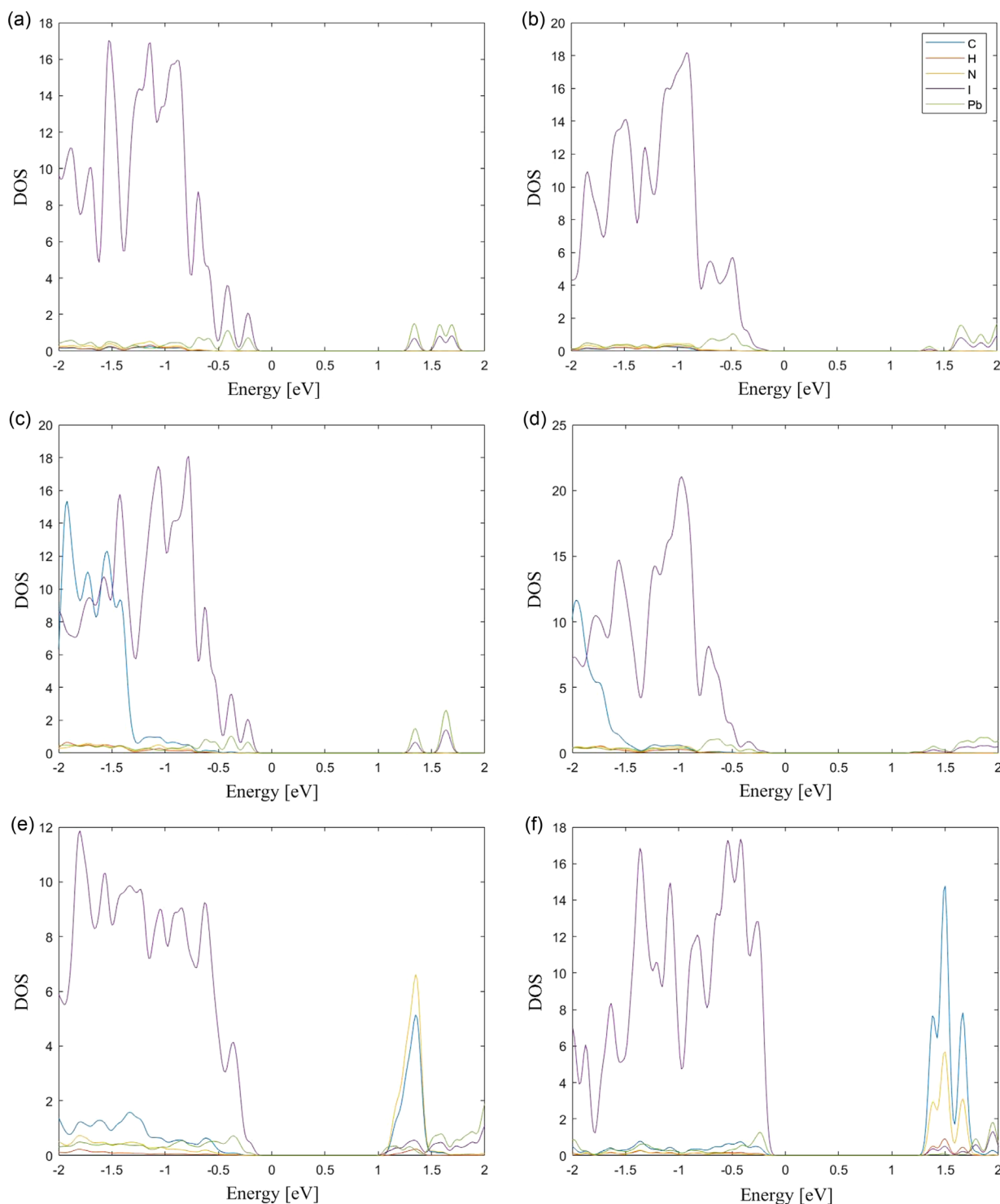


**Figure 7.** pDOS for an  $n = 1$  perovskite structure with a) BuA, b) BuDA, c) BnzA, d) BnzDA, e) IMI, and f) MP spacer molecules.

well with past studies of the relation between conjugation and electronic coupling in hybrid 2D perovskites.<sup>[35]</sup> We, therefore, explored this point further by calculating an additional system using 2-methylpyridinium (MP), which contains nitrogen in the ring. We analyzed its pDOS in the same manner, as shown in

Figure 7f. Clearly, a significant contribution of the organic molecule to the states at the gap edges arises also for the MP case, indicating that intrinsic gap states arise consistently only in the presence of  $N$  heteroatoms in the carbon ring. In the samples studied experimentally in this work, there are no  $N$

heteroatoms and therefore no intrinsic interface defect states are expected. This also agrees well with a previous study of adsorption of aryl vinyl derivatives on Si,<sup>[36]</sup> where the presence of an inner heteroatom was found to have a dominating effect on gap states at the Si/molecule interface. Obviously, the detailed chemistry of the MP case is entirely different than that explored in ref. [36], but the principle is similar.

We remind that for 3D methylammonium lead iodide (MAPI), iodine interstitials ( $I_i$ ) are considered to be detrimental recombination centers.<sup>[8,11]</sup> However, these defects are not expected to form recombination levels close to the conduction band,<sup>[11,15]</sup> unless their energetic position changes considerably in lower dimensions. Similar argument holds also for lead vacancies ( $V_{Pb}$ ) that are expected to form transition states far from the conduction band edge (at about mid-gap and closer to the valence band).<sup>[15]</sup> Iodine vacancies ( $V_I$ ), in contrast, are not considered as efficient recombination centers, as they are believed not to form an energy level deep within the energy gap of the bulk MAPI.<sup>[11,15]</sup> However, they do form a transition state very close to the conduction band of the 3D material.<sup>[15]</sup> This state could “move” into the energy gap of the 2D or quasi-2D material owing to changes in the energetic position of the conduction and valence bands. Similar considerations apply also to lead interstitials ( $Pb_i$ ) and MA interstitials ( $MA_i$ ).<sup>[15]</sup> However,  $Pb_i$  defects have a relatively high formation energy and are not expected to have a large density. In fact, Xiao et al.<sup>[17]</sup> found, using DFT calculations, that  $V_I$  in 2D  $(MA)_2Pb(SCN)_2I_2$  perovskite has a deep (0/1+) transition level at 0.40 eV below the conduction-band minimum (CBM). For  $MA_i$ , they calculated a shallow (0/1+) transition level at 0.14 eV below the CBM and a deep level, at 0.86 eV below the CBM for  $Pb_i$ . These values are expected to change with the dimensionality of the perovskite films when going to quasi-2D perovskites, as in the present case. Other defect states that are considered to form detrimental recombination centers are related to hydrogen vacancies ( $V_H$ ). Zhang et al.<sup>[8]</sup> addressed two types of such vacancies,  $V_H(N)$ —where a hydrogen atom was removed from a nitrogen atom and  $V_H(C)$ —where a hydrogen atom was removed from a carbon atom.

### 3. Conclusion

We studied the formation of in-gap states in quasi-2D lead-iodide-based perovskites, intercalated with various spacer molecules. We found, for all molecules used in this work, indications for the formation of shallow in-gap states, positioned at about 0.15–0.2 eV below the bottom of the conduction band. Moreover, our temperature-dependent photoconductivity measurements along with the theoretical fits to the SRH model suggest that these states are related to the dominant recombination route of the photogenerated carriers in those systems and have a relatively large capture coefficient of about  $10^{-5}$ – $10^{-6}$  cm<sup>3</sup> s<sup>-1</sup> at room temperature. DFT calculations imply that these states are not directly related to the inclusion of the spacer molecules. However, indirect effects of their inclusion, such as chemical modification of perovskite defects or structural deformation of the perovskite layers, are certainly possible. Our results suggest that further improvement of the performance of solar cells that are based on quasi-2D perovskites requires, along with

enhancing carrier mobility, further effort to suppress the concentration of detrimental defect states is needed.

### 4. Experimental Section

**Materials: Samples Fabrication:** Cover glasses (Paul Marienfeld) were cleaned stepwise in a sonication using Hellamnex, isopropanol, and a water–acetone–ethanol mixture. The clean substrates were dried and treated with oxygen plasma for 10 min, then directly moved to a nitrogen-filled glove box for the perovskite deposition; perovskite solution was dropped into the substrate, which was loaded for 10 s, and spin-coated at 1000 rpm (10 s), increasing to 5000 rpm (50 s). 30 s before the end of the spin, an antisolvent treatment was performed using 100  $\mu$ L of anhydrous chlorobenzene. The substrates were annealed for 30 min at 100 °C.

**Materials: Perovskite Solutions:** 1 M of perovskite solution was prepared by weighting stoichiometric ratio of spacer molecule, (MAI Greatcell), and lead iodide ( $PbI_2$  99.99% Merck), according to the relevant chemicals formula in a mixture of dimethylformaldehyde and dimethylsulfide (4:1).  $[(R-NH_3)_2(MA)_{n-1}Pb_nI_{3n+1}]$  for benzylammonium (BrzA), and butylammonium (BuA),  $[NH_3-R-NH_3](MA)_{n-1}Pb_nI_{3n+1}]$  for 1,4-butanediammonium (BuDA), and 1,4-benzenedimethan ammonium (BrzDA).

**Materials: Organic Spacer Synthesis:** Organic spacers were synthesized by careful reaction of alkylamines (benzylamine, butylamine, 1,4-Diaminobutane, 1,4-Benzenedimethanamine, Merck) with an excess of HI (57 wt% in H<sub>2</sub>O, distilled, stabilized, 99.95%, Merck), using a separatory funnel and round bottle flask. The product was left to stir for at least 30 min, and later washed from acid leftovers, recrystallized, and dried in a vacuum oven at 70 °C overnight.

**Characterization: Optical Characterizations:** Absorbance measurements were performed using a Jasco V-670 spectrophotometer. PL measurements were collected using HORIBA FluoroMax 4, where the light source is a continuous light source is 150-W ozone-free xenon arc lamp. The specific excitation wavelength was fixed by a monochromator.

**Characterization: STS:** Tunneling spectroscopy measurements were acquired using a home-built STM system supported by RHK electronics. All spectra were measured at room temperature, using a Pt–Ir tip. The tunneling current–voltage ( $I$ – $V$ ) characteristics were acquired using a tunneling current set point of 0.1 nA, while during the acquisition of the spectra the circuit feedback loop was momentarily disabled. The  $dI/dV$ - $V$  tunneling spectra, which are proportional to the local DOS, were numerically derived from the resulting curves by averaging over 5  $I$ – $V$  characteristics taken at a specific location, in each of which the current was recorded, and averaged over 64 times for every bias value.

**Characterization: Photoconductivity Measurements:** The temperature-dependent photoconductivity measurements were carried out using a liquid-N<sub>2</sub> flow optical-cryostat that enables monitoring and controlling the sample temperature using a Lakeshore temperature controller. We used Keithly 2400 SMU voltage source and a Digital Instruments 1211 current-amplifier connected to a Keithly 2100 DMM to probe the current through the sample. For illumination, we used a diode laser (658 nm) with maximum power of about 3.6 W. At every temperature, current–voltage ( $I$ – $V$ ) characteristics were measured in the dark and under illumination with different intensities, with a set of filters used to control the illumination intensity.

**Characterization: Hall Measurements:** Hall measurements were performed using a Lake Shore ac/dc Model 8404 Hall Effect system, using a high resistivity feature suitable for organic semiconductors. For the specific measurements, the samples were illuminated by a white LED source (0.25 Sun) and measured under a magnetic field of 1.7 T, and a current of 80 nA. Each measurement was conducted 10 times. The average results and the standard deviations were used to calculate the final values.

### Acknowledgements

D.A., O.M., and I.B. thank the support of ISF (grant no. 576/21). O.M. thanks the Harry de Jur, Chair in Applied Science. L.E. acknowledges

the Israel Ministry of Energy for its financial support. L.K. thanks the Minerva Centre for Self-Repairing Systems for Energy & Sustainability, the Aryeh and Mintzi Katzman Professorial Chair, and the Helen and Martin Kimmel Award for Innovative Investigation, for their support.

## Conflict of Interest

The authors declare no conflict of interest.

## Data Availability Statement

The data that support the findings of this study are available from the corresponding author upon reasonable request.

## Keywords

density functional theory calculations, halide perovskites, photoconductivity, scanning tunneling spectroscopy

Received: October 22, 2023

Revised: October 31, 2023

Published online:

- [1] X. Li, J. M. Hoffman, M. G. Kanatzidis, *Chem. Rev.* **2021**, *121*, 2230.
- [2] H. Tsai, W. Nie, J.-Ch. Blancon, C. C. Stoumpos, R. Asadpour, B. Harutyunyan, A. J. Neukirch, R. Verduzco, J. J. Crochet, S. Tretiak, L. Pedesseau, J. Even, M. A. Alam, G. Gupta, J. Lou, P. M. Ajayan, M. J. Bedzyk, M. G. Kanatzidis, A. D. Mohite, *Nature* **2016**, *536*, 312.
- [3] B. Cohen, T. Binyamin, T. Ben-Tzvi, O. Goldberg, A. Schlesinger, I. Balberg, O. Millo, E. Gross, D. Azulay, L. Etgar, *ACS Energy Lett.* **2022**, *7*, 217.
- [4] X. Li, J. Hoffman, W. Ke, M. Chen, H. Tsai, W. Nie, A. D. Mohite, M. Kepenekian, C. Katan, J. Even, M. R. Wasielewski, C. C. Stoumpos, M. G. Kanatzidis, *J. Am. Chem. Soc.* **2018**, *140*, 12226.
- [5] H. Lai, B. Kan, T. Liu, N. Zheng, Z. Xie, T. Zhou, X. Wan, X. Zhang, Y. Liu, Y. Chen, *Am. Chem. Soc.* **2018**, *140*, 11639.
- [6] G. Grancini, C. Roldán-Carmona, I. Zimmermann, E. Mosconi, X. Lee, D. Martineau, S. Narbey, F. Oswald, F. De Angelis, M. Graetzel, M. Khaja Nazeeruddin, *Nat. Commun.* **2017**, *8*, 15684.
- [7] B.-E. Cohen, M. Wierzbowska, L. Etgar, *Sustainable Energy Fuels* **2017**, *1*, 1935.
- [8] H. Xue, G. Brocks, S. Tao, *Phys. Rev. Mater.* **2022**, *6*, 055402.
- [9] C. Bao, F. Gao, *Rep. Prog. Phys.* **2022**, *85*, 096501.
- [10] X. Zhang, J.-X. Shen, M. E. Turiansky, C. G. Van de Walle, *Nat. Mater.* **2021**, *20*, 971.
- [11] X. Zhang, M. E. Turiansky, J.-X. Shen, C. G. Van de Walle, *Phys. Rev. B* **2020**, *101*, 140101(R).
- [12] M.-H. J. Du, *Phys. Chem. Lett.* **2015**, *6*, 1461.
- [13] M. Abdi-Jalebi, Z. Andaji-Garmaroudi, S. Cacovich, C. Stavrakas, B. Philippe, J. M. Richter, M. Alsari, E. P. Booker, E. M. Hutter, A. J. Pearson, S. Lilliu, T. J. Savenije, H. Rensmo, G. Divitini, C. Ducati, R. H. Friend, S. D. Stranks, *Nature* **2018**, *555*, 479.
- [14] W. S. Yang, B.-W. Park, E. H. Jung, N. J. Jeon, Y. C. Kim, D. U. Lee, S. S. Shin, J. Seo, E. K. Kim, J. H. Noh, S. Il Seok, *Science* **2017**, *356*, 1376.
- [15] D. Meggiolaro, S. G. Motti, E. Mosconi, A. J. Barker, J. Ball, C. A. R. Perini, F. Deschler, A. Petrozza, F. Di Angelis, *Energy Environ. Sci.* **2018**, *11*, 702.
- [16] D. R. Ceratti, A. Cohen, R. Tenne, Y. Rakita, L. Snarski, L. Cremonesi, I. Rosenhek-Goldian, I. Kaplan-Ashiri, T. Bendikov, V. Kalchenko, M. Elbaum, M. A. C. Potenza, L. Kronik, G. Hodes, D. Cahen, *Mater. Horiz.* **2021**, *8*, 1570.
- [17] Z. Xiao, W. Meng, J. Wang, Y. Yan, *Phys. Chem. Chem. Phys.* **2016**, *18*, 25786.
- [18] A. Fraccarollo, A. Zocante, L. Marchese, M. Cossi, *Phys. Chem. Chem. Phys.* **2020**, *22*, 20573.
- [19] A. Fraccarollo, L. Marchese, M. Cossi, *J. Phys. Chem. C* **2018**, *122*, 3677.
- [20] M. Perez, D. Ghosh, O. Prezhdo, W. Nie, S. Tretiak, A. Neukirch, *J. Phys. Chem. Lett.* **2022**, *13*, 5213.
- [21] A. Shpatz-Dayana, B.-E. Cohen, S. Aharon, C. Tenailleau, M. Wierzbowska, L. Etgar, *Chem. Mater.* **2018**, *30*, 8017.
- [22] D. Phuyal, M. Safdari, M. Pazoki, P. Liu, B. Philippe, K. O. Kvashnina, O. Karis, S. M. Butorin, H. Rensmo, T. Edvinsson, L. Kloo, J. M. Gardner, *Chem. Mater.* **2018**, *30*, 4959.
- [23] D. Azulay, I. Levine, S. Gupta, E. Barak-Kulbak, A. Bera, G. San, S. Simha, D. Cahen, O. Millo, G. Hodes, I. Balberg, *Phys. Chem. Chem. Phys.* **2018**, *20*, 24444.
- [24] N. Zakay, H. Stange, H. Alpern, D. Greiner, D. Abou-Ras, R. Mainz, I. Balberg, O. Millo, D. Azulay, *Phys. Rev. Appl.* **2020**, *14*, 024005.
- [25] R. H. Bube, *Photoelectronic Properties of Semiconductors*, Cambridge University Press, Cambridge, UK **1992**.
- [26] R. H. Bube, *Solid-State Electron.* **1984**, *27*, 467.
- [27] R. Cohen, L. Kronik, A. Shanzer, D. Cahen, A. Liu, Y. Rosenwaks, J. Lorenz, A. B. Ellis, *J. Am. Chem. Soc.* **1999**, *121*, 10545.
- [28] J. P. Perdew, K. Burke, M. Ernzerhof, *Phys. Rev. Lett.* **1996**, *77*, 3865.
- [29] T. Bucko, S. Lebegue, J. Hafner, J. G. Angyan, *J. Chem. Theory Comput.* **2013**, *9*, 4293.
- [30] T. Bucko, S. Lebegue, J. Hafner, J. G. Angyan, *J. Chem. Phys.* **2014**, *141*, 034114.
- [31] G. Kresse, J. Furthmüller, *Phys. Rev. B* **1996**, *54*, 169.
- [32] G. Kresse, D. Joubert, *Phys. Rev. B* **1999**, *59*, 1758.
- [33] W. H. Oswald, A. A. Koegel, J. R. Neilson, *Chem. Mater.* **2018**, *30*, 8606.
- [34] S. Kummel, L. Kronik, *Rev. Mod. Phys.* **2008**, *80*, 3.
- [35] Q. Dai, H. Li, G. Sini, J.-L. Bredas, *Adv. Funct. Mater.* **2022**, *32*, 2108662.
- [36] H. Alon, R. Garrick, S. P. Pujari, T. Toledano, O. Sinai, N. Klein-Kedem, T. Bendikov, J. Baio, T. Weidner, H. Zuilhof, D. Cahen, L. Kronik, C. N. Sukenik, A. Vilan, *J. Phys. Chem. C* **2018**, *122*, 3312.